

Effect of quintessence dark energy on the shadow of Hayward black holes with spherical accretion

Malihe Heydari-Fard *

Department of Physics, The University of Qom, 3716146611, Qom, Iran

March 10, 2023

Abstract

It is expected that the astrophysical black holes are surrounded by a luminous accretion flow that is a necessary ingredient for imaging a black hole. In this paper, we study the influence of quintessence dark energy on the shadow images of a Hayward black hole surrounded by the static/infalling spherical accretion flow. We find the effect of the state parameter of quintessence matter on the horizons, photon sphere and impact parameter of the quintessence Hayward black hole. The observed specific intensity of the shadow and also the shadow and photon ring luminosities of the quintessence Hayward black hole in two different spherically accretion flow are investigated. We also use the Event Horizon Telescope observational data of Sgr A* and M87* to constrain the free parameters of quintessence Hayward black hole. Finally, by comparison the results of quintessence Hayward black holes with quintessence Schwarzschild and Hayward black holes we find that the effect of quintessence matter on the black hole shadow is more significant than the regularity effect.

Keywords: Physics of black holes, Black hole shadow, Photon sphere, Spherical accretion, Modified theories of gravity

1 Introduction

The Event Horizon Telescope (EHT) collaboration has released Very Long Baseline Interferometry (VLBI) observations at the core of the M87 galaxy [1]–[6] and Milky Way galaxy [7] with angular resolution comparable to that expected of a supermassive black hole. The EHT images show a dark central area called the black hole shadow which is surrounded by a bright ring, the photon ring [8]. These results consistent with predictions of the theory of general relativity (GR) [9] and thus the EHT observations provide another strong evidence to Einstein’s theory. Synge was the first to investigate the deflection of light rays around a gravitationally intense star [10]. Bardeen then argued that the shadow radius of static Schwarzschild black hole is $r_s = 3M$, and also found that the angular momentum of rotating black holes deformed the shape of the shadow so that it’s not a perfect circle as the static case [11]. Moreover, in recent years many studies about the black hole shadow in the context of different space-time geometry have been done [12]–[27].

On the other hand, it is generally expected that the astrophysical black holes are not in an empty space but instead surrounded by an extremely luminous accretion flow which definitely affects the obtained image of the black hole. There are many papers and interesting discussions, show how the presence of accretion material modifies the black hole shadow. In 1979, Lunin extends the Synge’s work to a more realistic case in which the Schwarzschild black hole is surrounded by an accretion flow [28]. He studied the light deflection of a black hole surrounded by a geometrically thin, optically thick accretion disk and showed that the optical appearance of the black hole and the photon ring depend on both the location and profile of the accretion flow. In an interesting viewpoint, Gralla et al. by studying the properties of rings around black hole shadow of M87*

*Electronic address: heydarifard@qom.ac.ir

showed that depending on the intersection points of light rays with the plane of the disk there exist different rings called direct emission, lensing ring and photon ring. In this model, the accretion flow around the black hole is optically thin [29]. Moreover, the shadow of the Schwarzschild black hole surrounded by a geometrically thick, optically thin accretion flow has been studied by Cunha et al. in [30]. A simple spherical model of optically thin accretion in the space-time of the Schwarzschild black hole, and the study of properties of its shadow have been done in [31]. Narayan et al. argue that the behavior of the black hole image in spherical model is different from geometrically thin disk model, where the inner edge of the disk can leave an remarkable imprint on the image, especially when the edge of disk is out of the photon orbit. The shadow of quintessence Schwarzschild black hole surrounded by accretion flow for two types of the accretion flow, optically and geometrically thin disk accretion flow, and also spherically accretion flow, is studied in [32]. Authors have studied the effects of quintessence state parameter and accretion flow on the optical appearance of black hole [32]. Also, authors have studied the similar behavior for 4-dimensional Gauss-Bonnet black holes and explored the influence of both the Gauss-Bonnet parameter and spherical accretion flow on the properties of the black hole shadow [33]. The optical appearance of black holes in the context of Rastall gravity with different spherical accretions has been also studied in Ref. [34]. For further studies about the effect of the location and profile of accretion flow on the black hole shadow in alternative gravity theories see, [35]–[55].

The astronomical observations show that our universe is in an accelerated expansion phase caused by unknown component with negative pressure and positive energy density, is called dark energy [56]–[57]. One candidate interpret the negative pressure is the quintessence dark energy. The state equation of quintessence dark energy is $p = \omega\rho$ with ω being the quintessence state parameter in the range $-1 < \omega < -1/3$ [58]–[59]. The black hole solutions in the presence of quintessence dark energy have been extensively studied. The first static and spherically symmetric black hole solution containing the quintessence matter is obtained by Kiselev [60]–[61].

In addition to irregular black holes which have intrinsic singularity in the origin of space-time, black hole solutions without space-time singularity were first introduced by Bardeen [62]–[63] and later another type of regular black holes was presented by Hayward [64]. Rotating Hayward and charged Hayward black holes are also constructed in [65] and [66]. Similar to irregular black holes in the presence of quintessence matter, static Hayward black hole solution with quintessence matter has been obtained in [67]. The geodesic motion in the space-time of such a black hole is studied in [67]–[68] and extended to the rotating case in [69]. Also, for studying the shadow of rotating Hayward black holes in the absence and presence of quintessence matter see, [70]–[75]. However, the influence of quintessence matter on shadows and rings of Hayward black holes surrounded by spherical accretion flow has not yet been studied. So in the present work, similar to Ref. [32] we study the shadows and rings of Hayward black holes surrounded by spherical accretion, where the effects of quintessence state parameter on the optical appearance of black hole are investigated. We discuss the specific intensity of the shadow and the luminosities of the quintessence Hayward black hole shadow and photon ring, and also compare our results with the results corresponding to the Schwarzschild, quintessence Schwarzschild, and Hayward black holes.

The paper is structured as follows. In section 2, we present a brief review of Hayward black holes surrounded by quintessence matter and some of their properties. In section 3 we discuss the photon trajectories in the space-time of quintessence Hayward black holes and investigate the effect of the model parameters on them. In section 4 we present the shadow images of quintessence Hayward black hole with static and spherical accretion flow. The paper ends with drawing conclusions.

2 Hayward black holes with quintessence matter

The geometry of a Hayward black hole surrounded by quintessence dark energy can be expressed as [67]

$$ds^2 = -f(r)dt^2 + \frac{dr^2}{f(r)} + r^2 (d\theta^2 + \sin^2\theta d\varphi^2), \quad (1)$$

where

$$f(r) = 1 - \frac{2Mr^2}{r^3 + 2M\epsilon^2} - \frac{a}{r^{3\omega+1}}, \quad (2)$$

that M is the mass of black hole, ϵ is a parameter related to the cosmological constant and a and ω are the normalization factor and the state parameter of the quintessence matter, respectively. In Ref.[67] authors express the black hole mass, the radial distance and the parameter a in units of the ϵ , but here we define $2M\epsilon^2 \equiv g^3$ and investigate the effect of g parameter in our calculations. In the case of $a = 0$, the above metric reduces to the Hayward black hole obtained by Hayward [64], and for $\epsilon = 0$ represents the Schwarzschild black hole surrounded by quintessence matter that was initially obtained by Kiselev in [60]. Also, for $a = \epsilon = 0$ behaves like the Schwarzschild black hole that has only one event horizon. We also note by choosing different values of ω , the different black hole solutions can be obtained. For instance, when $\omega = -\frac{1}{3}$ the solution (1) corresponds to the Hayward black hole [64]. Moreover, in the case of $\omega = \frac{1}{3}$ and $a = -Q^2$ corresponds to the charged Hayward black hole [66].

The behavior of $f(r)$ function and thus the black hole horizons depend on the parameters g , a and ω . For quintessence dark energy the state parameter takes the values in the interval $-1 < \omega < -\frac{1}{3}$ and the energy density of quintessence matter is given by

$$\rho = -\frac{3\omega a}{2r^{3\omega+1}}. \quad (3)$$

As is clear, for a positive energy density the parameter a should be positive. In the present work, we take $\omega = -0.5$ and $\omega = -0.7$ and thus we investigate the behavior of horizons for two cases. The interested reader is referred to [67] for more discussions about properties of the black hole horizons. In what follows, we find the conditions that the Hayward metric surrounded by quintessence matter could have three horizons. From equation $f(r) = 0$ one can obtain the relationship between the black hole mass and the horizon radius as follows

$$M = \frac{r^3 + g^3}{2r^2} \left(1 - \frac{a}{r^{3\omega+1}}\right). \quad (4)$$

Choosing suitable values of the constants g , a and ω the function M is plotted in Fig. 1. It can be seen that the function M has a local maximum and minimum both located above the horizontal axis. For values of M in the interval $M_{\min} < M < M_{\max}$ the black hole has three horizons. The radii of inner and event horizons are represented by r_- and r_h respectively, while r_c is the cosmological horizon. There exist a critical value of normalization factor, a , for which $r_- = r_h = r_c$. This critical value a_{critical} is given by

$$a_{\text{critical}} = -\frac{4 + 3\omega + \sqrt{16 + 9\omega^2}}{2 - 3\omega + \sqrt{16 + 9\omega^2}} \left(\frac{\omega - 4 - \sqrt{16 + 9\omega^2}}{2\omega}\right)^{\omega+1/3} \frac{g^{3\omega+1}}{3\omega}, \quad (5)$$

when $a > a_{\text{critical}}$, there exist no black hole solution for any values of M , but in the case of $a < a_{\text{critical}}$ the black hole solutions exist for $M_{\min} < M < M_{\max}$.

In Table 1, we present the values of M_{\min} , M_{\max} for $a = 0.05$, $\omega = -0.7$ and different values of g . Also from equation (5) the value of a_{critical} is obtained for $\omega = -0.7$ and different values of g . In this work, we take $a = 0.05$, and $M = 1$ which is in interval M_{\min} and M_{\max} . In this case the value of a is smaller than a_{critical} for all values of g and thus we have the black hole solutions with three horizons.

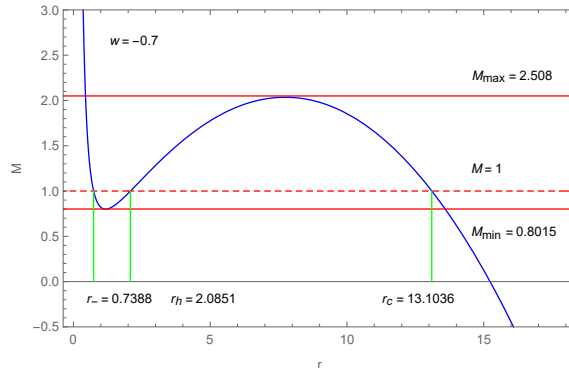


Figure 1: The black hole mass as a function of the radial coordinate r for $g = 0.9$, $a = 0.05$ and $\omega = -0.7$.

Table 1: The value of a_{critical} and also the values of M_{min} , M_{max} for $a = 0.05$, $\omega = -0.7$ and different values of g .

ω	g	a_{critical}	M_{min}	M_{max}
- 0.7	0.1	1.81558	0.47548	2.03223
- 0.7	0.3	0.54223	0.48783	2.03234
- 0.7	0.5	0.30914	0.45812	2.03277
- 0.7	0.7	0.21351	0.63224	2.03372
- 0.7	0.9	0.16194	0.80067	2.03540

The behavior of the function $f(r)$ for $M = 1$, $a = 0.05$ and $\omega = -0.7$ is plotted in Fig. 2. As the figure shows, $f(r)$ function has three real roots corresponding to r_- , r_h and r_c , respectively [67]. Also the difference between event horizon and the cosmic horizon decreases with the increases of absolute value of ω parameter, see Table 2.

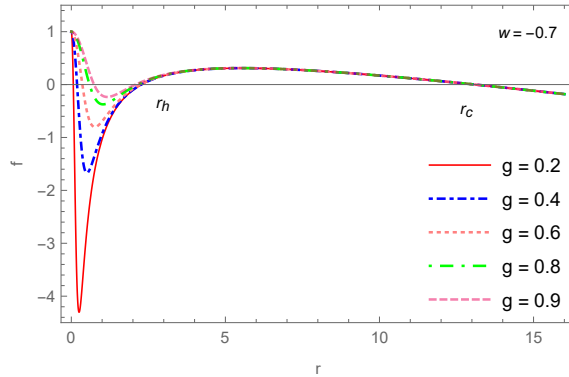


Figure 2: The metric coefficient $f(r)$ as a function of the radial coordinate r for $M = 1$, $a = 0.05$ and $\omega = -0.7$ with different values of g .

3 Light deflection by the quintessence Hayward black hole

To obtain the light deflection of quintessence Hayward black holes we study the null geodesics in the space-time of such black holes. Thus, we consider the Euler-Lagrange equation as follows

$$\frac{d}{ds} \left(\frac{\partial \mathcal{L}}{\partial \dot{x}^\mu} \right) - \frac{d\mathcal{L}}{dx^\mu} = 0, \quad (6)$$

where the Lagrangian density \mathcal{L} is given by

$$\mathcal{L} = \frac{1}{2} g_{\mu\nu} \dot{x}^\mu \dot{x}^\nu = \frac{1}{2} \left(-f(r) \dot{t}^2 + \frac{1}{f(r)} \dot{r}^2 + r^2 \dot{\theta}^2 + r^2 \sin^2 \theta \dot{\varphi}^2 \right), \quad (7)$$

\dot{x}^μ is the photon four-velocity, i.e., $\dot{x}^\mu = \frac{\partial x^\mu}{\partial s}$ where s denotes the affine parameter. For a spherically symmetric space-time without loss of generality, we consider the motion in the equatorial plane and impose two conditions $\theta = \frac{\pi}{2}$ and $\dot{\theta} = 0$. Also, since the metric coefficients have no explicit dependence on t and φ coordinates, there are two conserved quantities corresponding to the energy E and angular momentum L , of the photon. Now, using equations (2), (6) and (7) one can find

$$\dot{t} = - \frac{E}{1 - \frac{2Mr^2}{r^3 + g^3} - \frac{a}{r^{3\omega+1}}}, \quad (8)$$

$$\dot{\phi} = \frac{L}{r^2}, \quad (9)$$

$$\dot{r}^2 + \left(1 - \frac{2Mr^2}{r^3 + g^3} - \frac{a}{r^{3\omega+1}}\right) \left(\frac{L^2}{r^2} + h\right) = E^2, \quad (10)$$

where $h = 0$ and $h = 1$ correspond to the null-like and time-like geodesics, respectively. Considering the null geodesics with $h = 0$ and using equation (10), the effective potential can be rewrite as

$$V_{\text{eff}}(r) = \frac{L^2}{r^2} f(r) = \frac{L^2}{r^2} \left(1 - \frac{2Mr^2}{r^3 + g^3} - \frac{a}{r^{3\omega+1}}\right). \quad (11)$$

In Fig. 3, the effective potential of quintessence Hayward black holes is plotted for different values of the parameter g . The state parameter set to $\omega = -0.5$ and $\omega = -0.7$ in the left and right panels, respectively. It can be seen that increasing g leads to an increase in the peak of the potential, while with increasing the absolute value of ω the maximum of the potential decreases. The effect of quintessence parameter on the effective potential is displayed in Fig. 4, showing that in the presence of quintessence dark energy the maximum of the effective potential decreases, and for all values of g the peak of the potential for quintessence Hayward black holes is less than that for Hayward and Schwarzschild black holes.

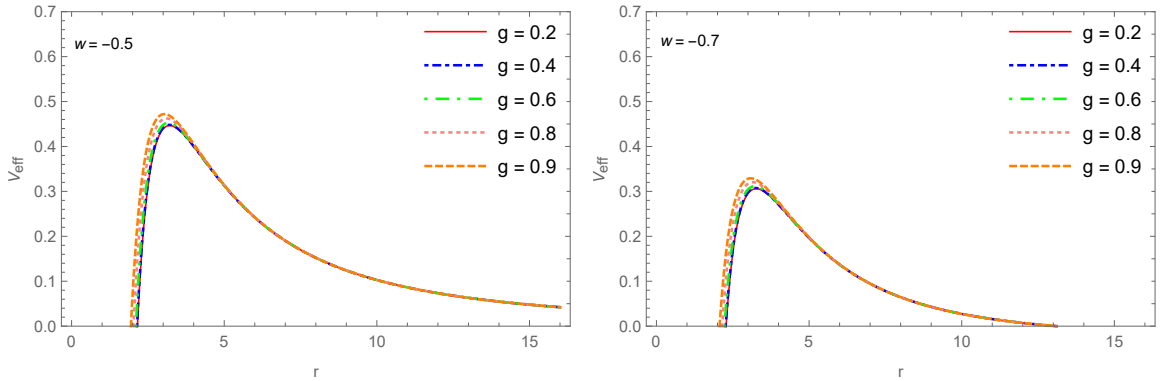


Figure 3: The effective potential as a function of the radial coordinate r for different values of g with $\omega = -0.5$ (left panel) and $\omega = -0.7$ (right panel) and $a = 0.05$.

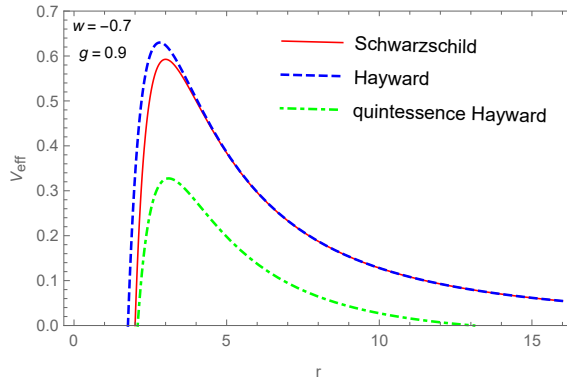


Figure 4: The effective potential as a function of the radial coordinate r for Schwarzschild space-time $g = a = 0$, Hayward black hole for $g = 0.9$, $a = 0$, and Hayward black hole surrounded by quintessence matter with $g = 0.9$, $a = 0.05$, $w = -0.7$ and $M = 1$.

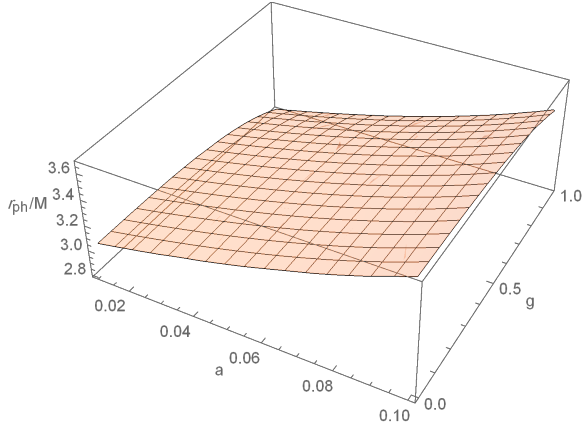


Figure 5: The behavior of the photon radius as a function of the parameters g and a for $\omega = -\frac{2}{3}$.

Now, we are going to obtain the photon sphere and impact parameter of photon sphere for quintessence Hayward black holes by employing the ray-tracing method. The photon orbit occurs at $r = r_{ph}$ and thus from equation (10) the conditions for such orbits are given by

$$V_{\text{eff}}(r_{ph}) = E_{ph}^2, \quad V'_{\text{eff}}(r_{ph}) = 0, \quad (12)$$

where the prime represents differentiation with respect to the radial coordinate r . Use of equation (11) leads to the following relation

$$r f'(r) - 2f(r) = 0. \quad (13)$$

Substituting $f(r)$ from equation (2) we obtain the following equation for the photon sphere

$$r^6 - 3mr^5 - 4g^3r^3 - 2g^6 + 3a(1 + \omega)(g^3 + r^3)^2r^{-(3\omega+1)} = 0, \quad (14)$$

which does not have an analytical solution and thus we numerically obtain the roots of that. For $a = g = 0$, we find $r_{ph} = 3M$ which is the photon radius for the Schwarzschild space-time. Also, in the case of $a = 0, g \neq 0$ namely for the Hayward black holes the above equation does not have an analytical solution while, for the Schwarzschild black holes in the presence of quintessence matter with $a \neq 0$ and $g = 0$ there is only an exact solution for $\omega = -\frac{2}{3}$ as follows

$$r_{ph} = \frac{1 - \sqrt{1 - 6Ma}}{a}. \quad (15)$$

Moreover, the impact parameter of the photon sphere defined as $b_{ph} = L_{ph}/E_{ph}$, is given by [76]

$$b_{ph} = \frac{r_{ph}}{\sqrt{f(r_{ph})}}. \quad (16)$$

The numerical results of the inner horizon radius r_- , event horizon r_h , cosmological horizon r_c , the radius of the photon sphere r_{ph} and the impact parameter of photon sphere b_{ph} for different values of g and ω with $M = 1$ and $a = 0.05$ are presented in Table 2. Cosmological horizon has an important role in the observed shadow of quintessence Hayward black holes, since we consider the distant observer nearby the cosmological horizon and the accretion flow near the event horizon. The difference between event horizon and cosmological horizon depends on quintessence state parameter ω and with increasing absolute value of ω , this difference decreases. When we fixed the value of ω and increased the g parameter, r_h , r_c , r_{ph} and b_{ph} decrease, however the rate of this decrease is very small for cosmic horizon r_c . We also see that for a fixed g with increasing the absolute value of ω the values of r_h and b_{ph} increase but the cosmological horizon r_c decreases. Moreover, the photon radius r_{ph} increases and then decreases around $\omega = -0.7$.

In Table 3, we compare the numerical values of r_h , r_c , r_{ph} and b_{ph} for the Schwarzschild space-time, Hayward black hole, quintessence Schwarzschild black hole and quintessence Hayward black hole. The first row

corresponds to the results of Schwarzschild black hole and the second row to those of Hayward regular black hole. The third and fourth rows correspond to the Schwarzschild and Hayward black holes surrounded by quintessence, respectively. The results of Table 3 on scales of the size of the horizons, photon sphere and impact parameter show that Hayward and quintessence Hayward black holes with a regular core do not significantly different from irregular Schwarzschild and quintessence Schwarzschild black hole, and seems unnecessary when other, more important ingredients such as quintessence background and accretion flow are present and presumably dominate.

For quintessence Hayward black holes under consideration, the dependence of the photon radius on the parameters a and g with $\omega = -\frac{2}{3}$ is plotted in Fig. 5. As the figure shows, for a fixed value of a with increasing g the photon radius decreases, while at fixed g by increasing a the photon radius increases. Also, it can be seen that for $a = g = 0$, $r_{ph} = 3M$ which is the radius of the photon sphere for the Schwarzschild black hole.

Table 2: The values of inner horizon, r_- , event horizon, r_h , cosmological horizon, r_c , photon radius, r_{ph} , and impact parameter, b_{ph} , for different values of g and ω , with $M = 1$, $a = 0.05$. The results in the first row of each ω corresponds to the quintessence schwarzschild black hole.

ω	g	r_-/M	r_h/M	r_c/M	r_{ph}/M	b_{ph}/M
- 0.4	0	—	2.1234	319999	3.1804	5.7295
	0.1	0.0222	2.1232	319999	3.1802	5.7293
	0.3	0.1177	2.1173	319999	3.1749	5.7246
	0.5	0.2623	2.0946	319999	3.1549	5.7064
	0.7	0.4586	2.0399	319999	3.1081	5.6646
	0.9	0.7298	1.9239	319999	3.0159	5.5844
- 0.5	0	—	2.1586	395.969	3.2163	5.9881
	0.1	0.0224	2.1584	395.969	3.2161	5.9879
	0.3	0.1187	2.1525	395.969	3.2109	5.9828
	0.5	0.2644	2.1299	395.969	3.1908	5.9635
	0.7	0.4618	2.0756	395.969	3.1439	5.9189
	0.9	0.7331	1.9610	395.969	3.0518	5.8335
- 0.6	0	—	2.2080	39.6448	3.2504	6.4204
	0.1	0.0224	2.2078	39.6448	3.2502	6.4201
	0.3	0.1192	2.2019	39.6448	3.2449	6.4142
	0.5	0.2658	2.1794	39.6448	3.2246	6.3919
	0.7	0.4643	2.1252	39.6448	3.1772	6.3403
	0.9	0.7361	2.0115	39.6448	3.0841	6.2498
- 0.7	0	—	2.2830	13.1027	3.2710	7.2343
	0.1	0.2246	2.2828	13.1027	3.2708	7.2340
	0.3	0.1194	2.2769	13.1028	3.2654	7.2259
	0.5	0.2665	2.2539	13.1029	3.2446	7.1952
	0.7	0.4656	2.1992	13.1031	3.1961	7.1245
	0.9	0.7379	2.0851	13.1036	3.1007	6.9900
- 0.8	0	—	2.4149	6.5509	3.2548	9.2206
	0.1	0.0225	2.4146	6.5509	3.2546	9.2199
	0.3	0.1198	2.4083	6.5513	3.2489	9.2027
	0.5	0.2674	2.3839	6.5523	3.2275	9.1375
	0.7	0.4678	2.3262	6.5547	3.1773	8.9892
	0.9	0.7413	2.2075	6.5587	3.0784	8.7135

Table 3: The values of event horizon, r_h , cosmological horizon, r_c , photon radius, r_{ph} , and impact parameter, b_{ph} , for Schwarzschild space-time, Hayward black hole, Schwarzschild and Hayward black holes surrounded by quintessence matter.

<i>Type</i>	ω	a	g	r_h/M	r_c/M	r_{ph}/M	b_{ph}/M
Schwarzschild	–	0	0	2	–	3	5.19615
Hayward	–	0	0.5	1.96772	–	2.97162	5.17169
Quintessence Schwarzschild	- 0.5	0.05	0	2.15857	395.9690	3.21631	5.98805
Quintessence Hayward	- 0.5	0.05	0.5	2.12987	395.9690	3.19078	5.96347

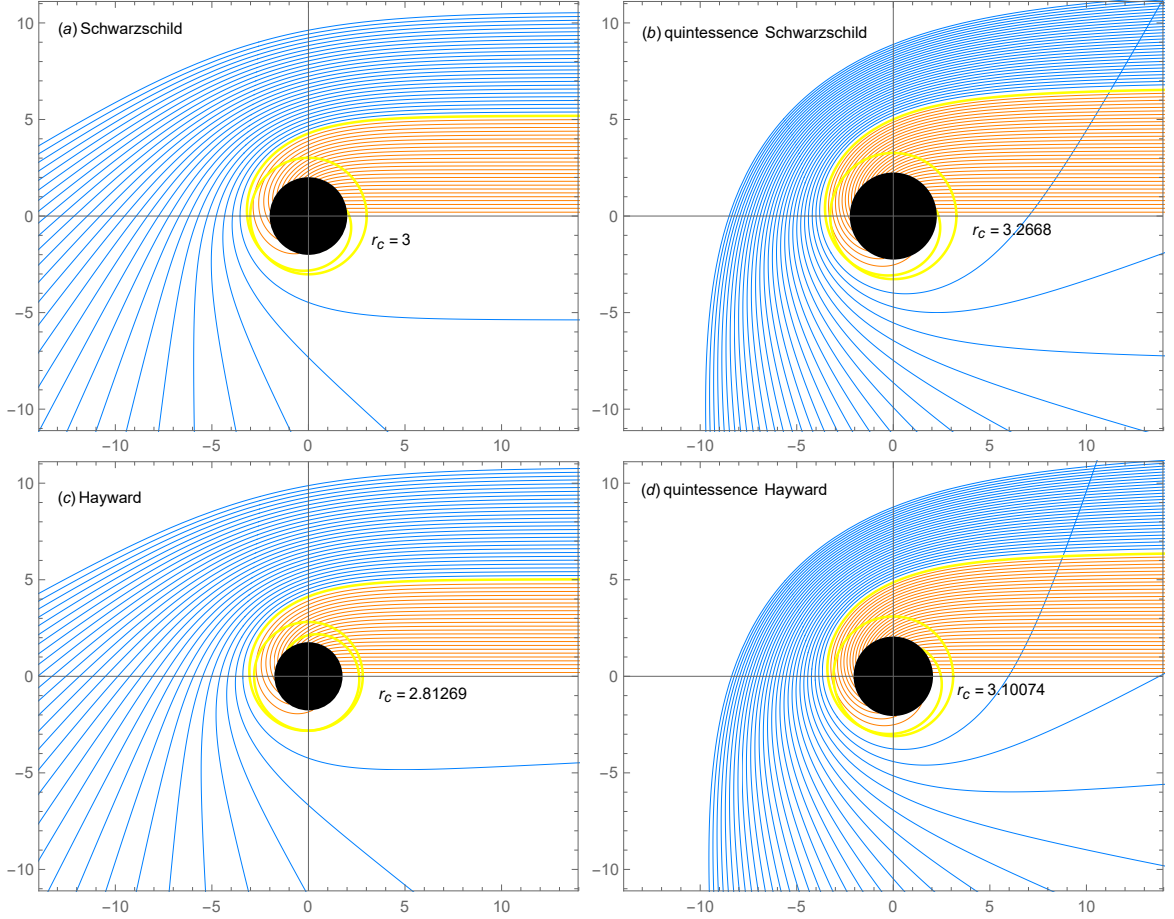


Figure 6: The polar plot of light rays around a schwarzschild black hole with and without quintessence matter (top row) and a Hayward black hole with and without quintessence matter (bottom row) for $g = 0.9$ and $a = 0.05$, $\omega = -0.7$ with $M = 1$. The yellow, blue and orange curves correspond to the trajectory of light rays with $E = E_{ph}$, $E < E_{ph}$ and $E > E_{ph}$, respectively.

Using equations (9) and (10) and new variable $u = \frac{1}{r}$ we find

$$\frac{du}{d\varphi} = \sqrt{\frac{1}{b^2} - u^2 \left(1 - \frac{2Mu}{1 + g^3 u^3} - au^{3\omega+1} \right)}. \quad (17)$$

Assuming that light rays approach the black hole from the right side, shadow and photon sphere are formed from the deflection of light corresponds to the Fig. 6. The light trajectories in the space-time of Schwarzschild,

quintessence Schwarzschild, Hayward and quintessence Hayward black holes are plotted in panels (a) to (d). As can be seen, by increasing the parameter g the shadow radius decreases, while in the presence of quintessence matter an enhancement in the absolute value of ω , increases the shadow radius which is in agreement with Table 2. The top row shows the results of the Schwarzschild and quintessence Schwarzschild black holes while the bottom row shows the results of regular Hayward black holes in the absence and presence of quintessence matter. By comparing figures (a) with (c) and also (b) with (d), we find that by increasing the parameter g the light deflection is smaller, namely the presence of the parameter g cause to decrease the strength of the gravitational field and thus diminishes the light bending angle [77]. On the other hand, comparing the results of figures (a) with (b) and also results of (c) with (d) show that the presence of quintessence matter increases the deflection of light rays [78].

Since the shadow is the fingerprint of the metric of space-time, one can constrain the parameter of the space-time geometry by the observed shadow [79]-[86]. The angular diameter Ω of the black hole shadow for a distant observer can be defined as [79]

$$\Omega = \frac{2b_{ph}}{D}, \quad (18)$$

where D is the distance between the black hole and distant observer. Equation (18) can be rewritten as

$$\left(\frac{\Omega}{\mu as} \right) = \left(\frac{6.191165 \times 10^{-8}}{\pi} \frac{\gamma}{D/Mpc} \right) \left(\frac{b_{ph}}{M} \right), \quad (19)$$

here γ is the mass ratio of the black hole to the Sun and the impact parameter of the photon sphere, b_{ph} , is obtained from equation (16).

For quintessence Hayward black hole, one can obtain the constraints of the free parameters using the shadow diameter estimated by the EHT observations. We consider the quintessence Schwarzschild black hole ($g = 0$) with $\omega = -2/3$ and constrain parameter a for both M87* and Sagittarius A* in Fig. 7. Current observations correspond to $\gamma = 4.14 \times 10^6$, and distance $D = 8.127$ kpc for Sagittarius A* and $\gamma = 6.2 \times 10^9$, and distance $D = 16.8$ Mpc for M87*, respectively [1]-[7]. The yellow and pink regions are the shadow diameters of M87* ($42 \pm 3 \mu as$) and Sagittarius A* ($51.8 \pm 2.3 \mu as$) reported by the EHT observations. Consequently, we constrain the parameter a of the quintessence Schwarzschild black hole as $0.007 < a < 0.033$ for M87*, and $0 < a < 0.0078$ for Sagittarius A*.

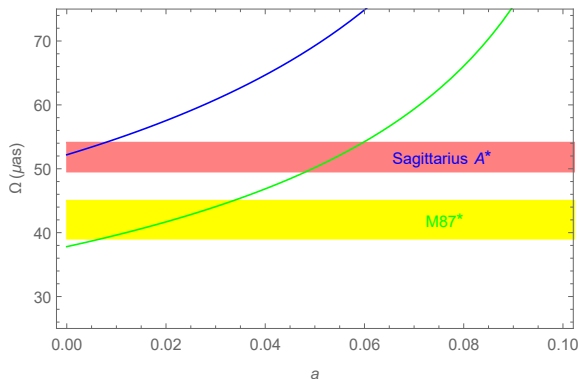


Figure 7: The relation between the angular diameter Ω of the observed shadow and the parameter a for a quintessence Schwarzschild black hole with $w = -2/3$. The pink and yellow regions are the experimental data of Sagittarius A* ($51.8 \pm 2.3 \mu as$) and M87* ($42 \pm 3 \mu as$) and reported by the EHT, respectively.

4 Shadows and photon rings with spherical accretion flow

Now, we are going to study the optical appearance of Hayward black hole surrounded by the quintessence matter with the spherical accretion flow and investigate the influence of the parameter g , and quintessence state

parameter, ω , on it. First, we consider a static spherical accretion model of optically and geometrically thin accretion flows and then focus on infalling spherical accretion flows.

4.1 The static spherical accretion

First we investigate the shadow and photon ring in the background of a quintessence Hayward black hole surrounded by static spherical accretion flow. The observed specific intensity can be obtained by integrating the specific emissivity along any ray path [87]–[88]

$$I(\nu_{\text{obs}}) = \int_{\gamma} g^3 j(\nu_{\text{em}}) dl_p, \quad (20)$$

with

$$g \equiv \frac{\nu_{\text{obs}}}{\nu_{\text{em}}}. \quad (21)$$

In the above equation, g is the redshift factor, while ν_{obs} and ν_{em} denote the observed photon frequency and radiated photon frequency, respectively. In the quintessence Hayward black hole space-time (1), the redshift factor is $g = f(r)^{1/2}$. Assuming that the emission is monochromatic with rest frame frequency ν_t and the emission radial profile is $1/r^2$ [88], the specific emissivity takes the form

$$j(\nu_{\text{em}}) \propto \frac{\delta(\nu_{\text{em}} - \nu_t)}{r^2}. \quad (22)$$

Also, according to equation (1), the proper length measured in the rest frame of the emitter is given by

$$dl_p = \sqrt{\frac{1}{f(r)} dr^2 + r^2 d\varphi^2} = \sqrt{\frac{1}{f(r)} + r^2 \left(\frac{d\varphi}{dr}\right)^2} dr. \quad (23)$$

Thus, by substituting equation (17) into equation (23), we obtain the specific intensity observed by a distant observer as

$$I(\nu_{\text{obs}}) = \int_{\gamma} \frac{f(r)}{r^2} \sqrt{1 + \frac{b^2 f(r)}{r^2 - b^2 f(r)}} dr. \quad (24)$$

From equation (17), it is clear that the trajectory of light rays depends on impact parameter b , so that in the case of $b = b_{ph}$, ($E = E_{ph}$), the photons will revolve around the black hole several times and for $b > b_{ph}$, ($E < E_{ph}$), the light rays deflect by it. Moreover, the photons with $b < b_{ph}$, ($E > E_{ph}$), eventually fall into the black hole singularity. Therefore, in order to study the photon intensity which associate with the light trajectories, we plotted the observed intensity as a function of impact parameter b . In Fig. 8, the plots of intensity as a function of b for different values of the parameter g , with $\omega = -0.5$ (left panel) and $\omega = -0.7$ (right panel) are presented. Clearly, the intensity increases with impact parameter, sharply peak at $b = b_{ph}$ and then decreases with b . The reason for maximum intensity at $b = b_{ph}$ is that the photon revolves around the black hole several times as it approaches the photon sphere. Meanwhile, at fixed ω the peak value of intensity increases with increasing g so that the quintessence Schwarzschild black hole with $g = 0$ has the smallest value. Also, for a given value of g the larger absolute value of ω has the smaller intensity, namely the case of $\omega = -0.7$ has the smaller intensity in comparison with $\omega = -0.5$. It shows that in the presence of quintessence dark energy the observed intensity decreases.

Shadows and photon rings of quintessence Hayward black holes for different values of g with $\omega = -0.5$ and $\omega = -0.7$ are shown in Fig. 9. It is clear that for a fixed value of ω with increase of g , the radius of shadows and photon rings of quintessence Hayward black holes decrease while their luminosity increases, so that the quintessence Schwarzschild black hole with $g = 0$ has the lowest luminosity in comparison with quintessence Hayward black holes. This is due to the fact that the gravitational field of quintessence Schwarzschild black hole with $g = 0$ is stronger which increases the light deflection and leads to more photons being trapped by the black hole and a lower luminosity of shadow and photon ring being observed compared to quintessence Hayward

black holes. Also, comparing plots in the top row of the figure with those in the bottom row shows the effect of the state parameter of the quintessence matter ω on the black hole shadow and photon ring; for a fixed value of g the luminosity of the photon ring increase with the absolute value of ω .

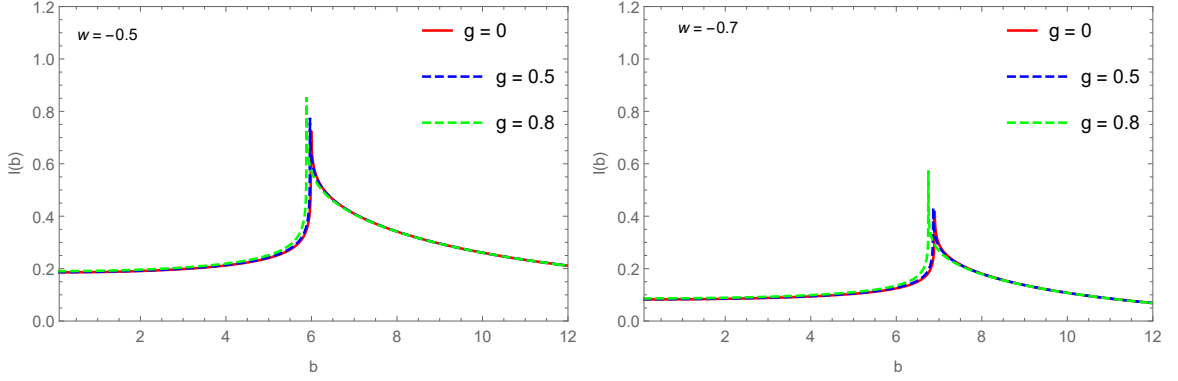


Figure 8: The observed intensity $I(\nu_{\text{obs}})$ for static spherical accretion flow around a quintessence Hayward black hole $\omega = -0.5$ (left panel) and $\omega = -0.7$ (right panel) for different value of g , $a = 0.05$ and $M = 1$.

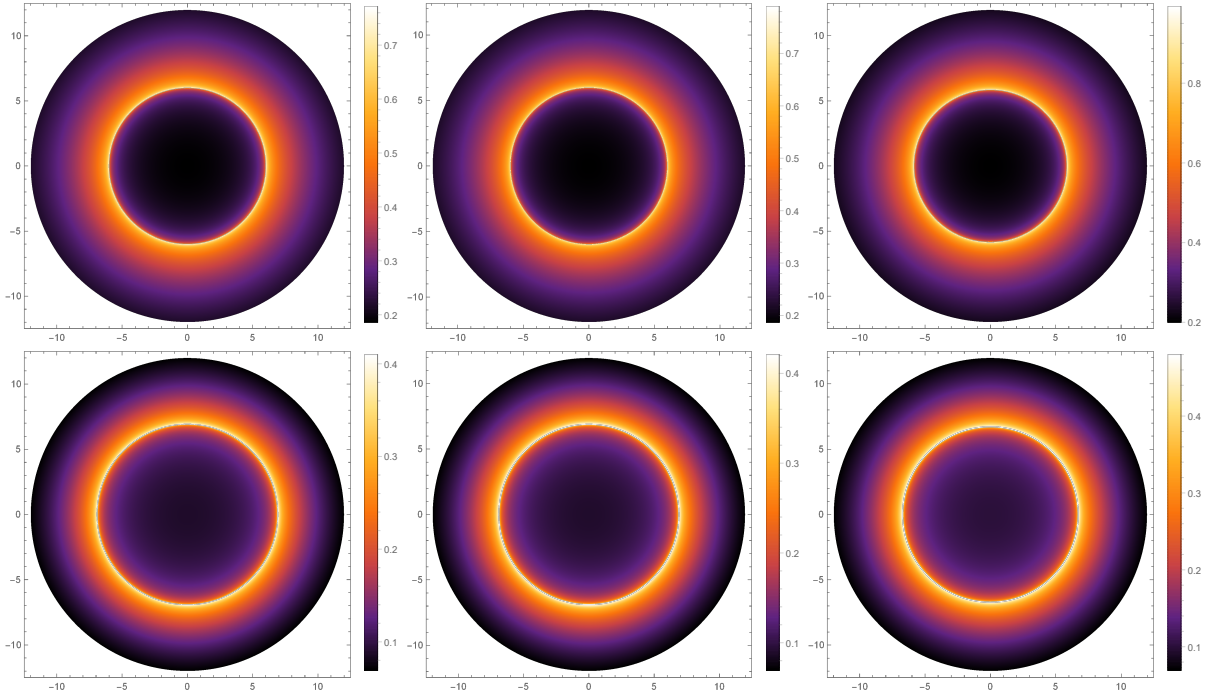


Figure 9: Shadows and photon rings for static spherical accretion flow, $\omega = -0.5$ (top row) and $\omega = -0.7$ (bottom row) for different values of g , $a = 0.05$ and $M = 1$. The parameter g from left to right is 0, 0.5 and 0.8, respectively.

4.2 The infalling spherical accretion

Since in our real universe the most of accretions are moving, in this section we consider the black hole shadows and photon rings in the context of infalling spherical accretion. Note that the observed intensity for a distant

observer in the case of infalling spherical accretion is still expressed as equation (24), but the redshift factor is different from static model and is related to the velocity of accretion flow

$$g = \frac{k_\alpha u_{\text{obs}}^\alpha}{k_\beta u_{\text{em}}^\beta}, \quad (25)$$

where $k^\mu \equiv \dot{x}^\mu$, $u_{\text{obs}}^\mu = (1, 0, 0, 0)$ and u_{em}^μ are the photon four-velocity, distant observer four-velocity and accretion four-velocity, respectively. From equation (8) we know that $k_t = 1/b$ is a constant and k_r can be obtained from condition $k_\mu k^\mu = 0$. Therefore, we find

$$\frac{k_r}{k_t} = \pm \sqrt{\frac{1}{f(r)} \left(\frac{1}{f(r)} - \frac{b^2}{r^2} \right)}, \quad (26)$$

where the upper and lower sign denote to the case that the photons approach or away from the black hole, respectively. The four-velocity of the infalling accretion is $(u_{em}^t, u_{em}^r, u_{em}^\theta, u_{em}^\varphi) = (\frac{1}{f(r)}, -\sqrt{1-f(r)}, 0, 0)$. Using these equations, the redshift factor in equation (25) can be obtained as

$$g = \frac{1}{u_{em}^t + \left(\frac{k_r}{k_t}\right) u_{em}^r}. \quad (27)$$

Moreover, the proper distance is defined as

$$dl_p = k_\alpha u_{em}^\alpha ds = \frac{k_t}{g^3 |k_r|} dr, \quad (28)$$

where s is the affine parameter along the photon path. By assuming that the specific emissivity is monochromatic the specific intensity $I(\nu_{\text{obs}})$ in the case of infalling spherical accretion thus can be written as

$$I = \int \frac{g^3}{r^2 \sqrt{\frac{1}{f(r)} \left(\frac{1}{f(r)} - \frac{b^2}{r^2} \right)}} dr. \quad (29)$$

The observed intensity with respect to parameter b with $\omega = -0.5$ (left panel) and $\omega = -0.7$ (right panel) is plotted in Fig. 10. It is easy to see that the behavior of intensity is similar to the case of static spherical accretion flow and peak is at b_{ph} , but the maximum of intensity in this case is less than that of static case.

Image of shadow cast for $\omega = -0.5$ and $\omega = -0.7$ are shown in Fig. 11. Clearly, in both cases at fixed ω with increasing parameter g , luminosity of shadows and photon rings increase. Moreover, by comparing plots in the top row of the figure with those in the bottom row we find that at a given g , for instance $g = 0.8$, the radius of shadows and photon rings and their luminosities increase with the absolute value of state parameter. Note that the properties of the black hole shadows and photon ring not only depend on the space-time geometry but also on the accretion flow property. In the other words, the radius of shadows and photon rings do not change in the case of static and infalling spherical accretion, but we find that the specific intensity of static accretion is higher than that of infalling accretion for the same parameters ω and g , resulting in the central shadow region for the infalling accretion is darker than that for static accretion which is caused by the Doppler effect in this case. Finally, the observed intensity in the space-times of Schwarzschild black hole, Hayward and quintessence Hayward black holes has been compared in the left and right panels of Fig. 12 for static and infalling cases, respectively.

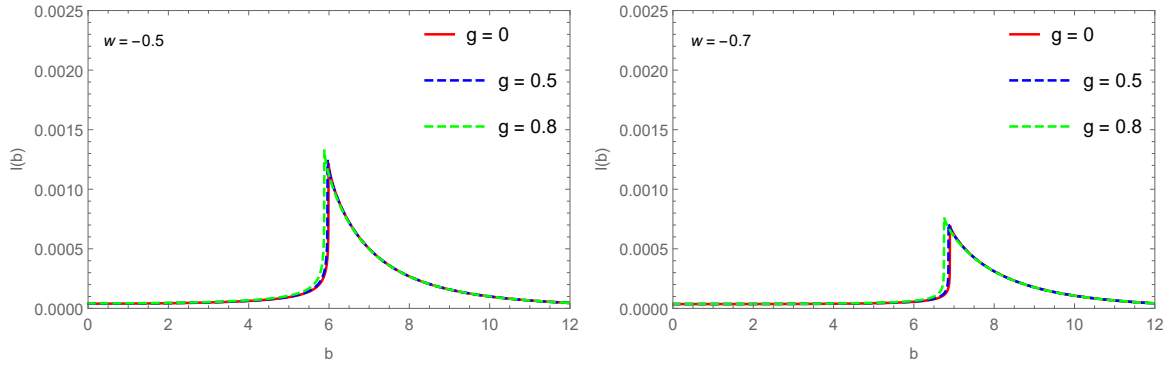


Figure 10: The observed intensity $I(\nu_{\text{obs}})$ for infalling spherical accretion flow around a quintessence Hayward black hole $\omega = -0.5$ (left panel) and $\omega = -0.7$ (right panel) for different value of g , $a = 0.05$ and $M = 1$.

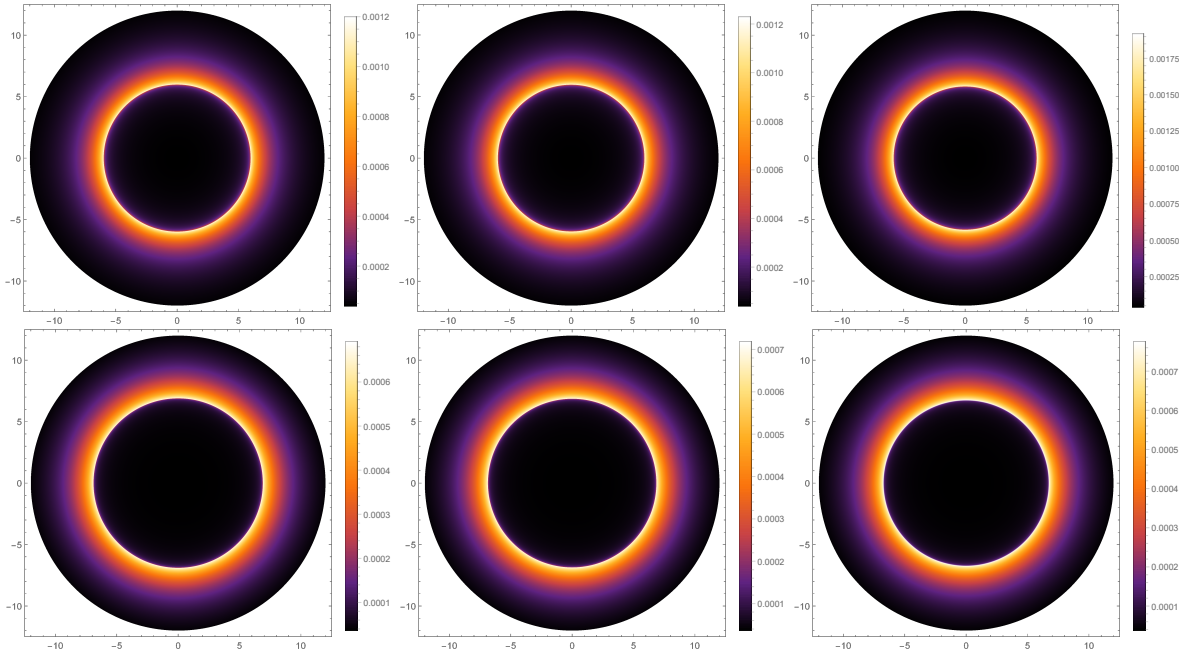


Figure 11: Black hole shadows and photon rings for infalling spherical accretion flow, $\omega = -0.5$ (top row) and $\omega = -0.7$ (bottom row) for different value of g , $a = 0.05$ and $M = 1$. The parameter g from left to right is 0, 0.5 and 0.8, respectively

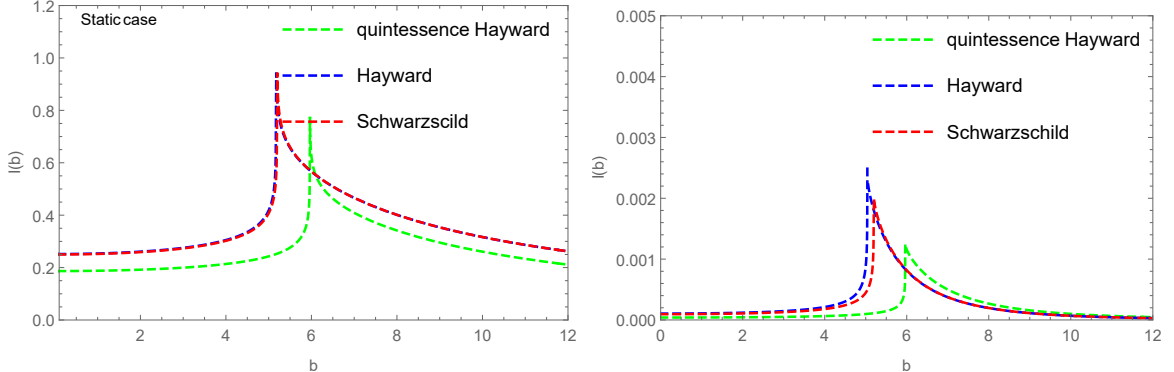


Figure 12: The observed intensity $I(\nu_{\text{obs}})$ for static (left panel) and infalling (right panel) spherical accretion flow around a Schwarzschild, Hayward and quintessence Hayward black hole for $g = 0.9$, $a = 0.05$ and $M = 1$.

5 Conclusions

Shadows and observational appearance of quintessence Schwarzschild black hole surrounded by various profiles of accretion flow has been studied in [32]. On the other hand the analysis of null geodesics for quintessence Hayward black hole (without accretion flow) is explored in [67]. In this paper, we considered quintessence Hayward black hole solution [67] surrounded by the static/infalling spherical accretion and similar to Ref. [32] investigated the effect of accretion flow on the optical appearance of this black hole. First, we discussed the event horizon properties of quintessence Hayward black hole. We calculated the numerical values of the inner horizon r_- , event horizon r_h , cosmological horizon r_c , the radius of the photon sphere r_{ph} , and impact parameter of the photon sphere b_{ph} for various values of g and ω , with the results summarized in Table 2. According to Table 2 for a fixed ω with increasing g the values of r_{ph} and b_{ph} decrease, while at fixed g when we increase the absolute value of ω , the values of r_{ph} and b_{ph} increases too. Photon trajectories in the vicinity of this black hole for different values of energy are plotted and showed the presence of quintessence matter increases the deflection of light rays, while the parameter g oppositely effects the behavior of light deflection. We also constrained the amount of the free parameter of the quintessence Schwarzschild black hole with $\omega = -0.7$ compatible with the EHT observations of Sgr A* and M87* supermassive black holes.

Furthermore, we assumed that quintessence Hayward black hole surrounded by spherical accretion flow and considered two relativistic models: the static and infalling spherical accretion flow. Then, in Fig. 8 and Fig. 10 we plotted the profile of observed intensity as a function of impact parameter for $\omega = -0.5$ and $\omega = -0.7$ with different values of g , in the model with gas at rest and, in radially infalling gas accretion scenario, respectively. Shadows and photon rings for $\omega = -0.5$ and $\omega = -0.7$ with different values of g are also shown in Fig. 9 and Fig. 11. The size of shadows and photon rings decrease and their intensity and luminosity increase for a fixed ω with increasing g , while the effect of the absolute value of ω is opposite. For a fixed ω with decreasing g , the strength of the gravitational field around the black hole increases and so the impact parameter increases and more photons capture by the black hole (tiny fraction of photons escape from black hole), and so a lower luminosities of shadows and photon rings being observed. Also, the results of quintessence Hayward black holes shows that the effect of quintessence background on the size of the black hole shadow, photon rings and their luminosities is more significant in comparison with that for Hayward black holes while, the comparison between quintessence Schwarzschild and quintessence Hayward black holes shows that the regularity faintly affects the shadow size, photon rings and their luminosities. Finally, it is worth noting that the realistic black holes rotate so we will extend this static solution to kerr-like solution in future.

Data Availability

Data sharing not applicable to this article as no datasets were generated or analysed during the current study.

References

- [1] K. Akiyama, et al. *First M87 event horizon telescope results. I. The shadow of the supermassive black hole*, *Astrophys. J.* **875** (2019) L1 <https://dx.doi.org/10.3847/2041-8213/ab0ec7>.
- [2] K. Akiyama, et al. *First M87 Event Horizon Telescope Results. II. Array and Instrumentation*, *Astrophys. J.* **875** (2019) L2 <https://dx.doi.org/10.3847/2041-8213/ab0c96>.
- [3] K. Akiyama, et al. *First M87 Event Horizon Telescope Results. III. Data Processing and Calibration*, *Astrophys. J.* **875** (2019) L3 <https://dx.doi.org/10.3847/2041-8213/ab0c57>.
- [4] K. Akiyama, et al. *First M87 Event Horizon Telescope Results. IV. Imaging the Central Supermassive Black Hole*, *Astrophys. J.* **875** (2019) L4 <https://dx.doi.org/10.3847/2041-8213/ab0e85>.
- [5] K. Akiyama, et al. *First M87 Event Horizon Telescope Results. V. Physical Origin of the Asymmetric Ring*, *Astrophys. J.* **875** (2019) L5 <https://dx.doi.org/10.3847/2041-8213/ab0f43>.
- [6] K. Akiyama, et al. *First M87 Event Horizon Telescope Results. VI. The Shadow and Mass of the Central Black Hole*, *Astrophys. J.* **875** (2019) L6 <https://dx.doi.org/10.3847/2041-8213/ab1141>.
- [7] K. Akiyama, A. Alberdi, W. Alef, J.C. Algaba and R. Anantua, *First Sagittarius A* Event Horizon Telescope Results. I. The Shadow of the Supermassive Black Hole in the Center of the Milky Way*, *Astrophys. J. Letter.* **930** (2022) L12 <https://dx.doi.org/10.3847/2041-8213/ac6674>.
- [8] P.V.P. Cunha and C.A.R. Herdeiro, *Shadows and strong gravitational lensing: a brief review*, *Gen. Relativ. Grav.* **50** (2018) 42 <https://doi.org/10.1007/s10714-018-2361-9>.
- [9] R.M. Wald, *General Relativity* (The University of Chicago Press, 1984).
- [10] J.L. Synge, *The Escape of Photons from Gravitationally Intense Stars*, *Mon. Not. R. Astron. Soc.* **131** (1966) 463 <https://doi.org/10.1093/mnras/131.3.463>.
- [11] J.M. Bardeen, in *Black holes, in Proceeding of the Les Houches Summer School, Session 215239* edited by De Witt, C., De Witt, B.S., (Gordon and Breach, NewYork, 1973).
- [12] L. Amarilla, E.F. Eiroa and G. Giribet, *Null geodesics and shadow of a rotating black hole in extended Chern-Simons modified gravity*, *Phys. Rev. D* **81** (2010) 124045 <https://doi.org/10.1103/PhysRevD.81.124045>.
- [13] F. Atamurotov, A. Abdujabbarov and B. Ahmedov, *Shadow of rotating Horava-Lifshitz black hole*, *Astrophys. Space Sci.* **348** (2013) 179 <https://doi.org/10.1007/s10509-013-1548-5>.
- [14] A. Abdujabbarov, F. Atamurotov, N. Dadhich, B. Ahmedov and Z. Stuchlik, *Energetics and optical properties of 6-dimensional rotating black hole in pure Gauss-Bonnet gravity*, *Eur. Phys. J. C* **75** (2015) 399 <https://doi.org/10.1140/epjc/s10052-015-3604-5>.
- [15] P.V.P. Cunha, C.A.R. Herdeiro, B. Kleihaus, J. Kunz and E. Radu, *Shadows of Einstein-dilaton-Gauss-Bonnet black holes*, *Phys. Lett. B* **768** (2017) 373 <https://doi.org/10.1016/j.physletb.2017.03.020>.
- [16] B.P. Singh and S.G. Ghosh, *Shadow of Schwarzschild-Tangherlini black holes*, *Ann. Phys* **395** (2018) 127 <https://doi.org/10.1016/j.aop.2018.05.010>.
- [17] S. Vagnozzi and L. Visinelli, *Hunting for extra dimensions in the shadow of M87**, *Phys. Rev. D* **100** (2019) 024020 <https://doi.org/10.1103/PhysRevD.100.024020>.
- [18] G.Z. Babar, A.Z. Babar and F. Atamurotov, *Optical properties of Kerr-Newman spacetime in the presence of plasma*, *Eur. Phys. J. C* **80** (2020) 761 <https://doi.org/10.1140/epjc/s10052-020-8346-3>.

- [19] I. Banerjee, S. Chakraborty and S. Sen Gupta, *Silhouette of M87*: A new window to peek into the world of hidden dimensions*, *Phys. Rev. D* **101**, (2020) 041301 <https://doi.org/10.1103/PhysRevD.101.041301>.
- [20] M. Khodadi and E.N. Saridakis, *Einstein-aether gravity in the light of event horizon telescope observations of M87**, *Phys. Dark. Univ* **32** (2021) 100835 <https://doi.org/10.1016/j.dark.2021.100835>.
- [21] M. Khodadi, G. Lambiase and D.F. Mota, *No-hair theorem in the wake of Event Horizon Telescope*, *JCAP* **09** (2021) 028 <https://dx.doi.org/10.1088/1475-7516/2021/09/028>.
- [22] J. Badia and E.F. Eiroa, *Shadow of axisymmetric, stationary, and asymptotically flat black holes in the presence of plasma*, *Phys. Rev. D* **104** (2021) 084055 <https://doi.org/10.1103/PhysRevD.104.084055>.
- [23] M. Okyay and A. Ovgun, *Nonlinear electrodynamics effects on the black hole shadow, deflection angle, quasi-normal modes and greybody factors*, *JCAP* **01** (2022) 009 <https://doi.org/10.1088/1475-7516/2022/01/009>.
- [24] F.Rahaman, K.N. Singh, R.Shaikh, T. Manna and S. Aktar, *Shadows of Lorentzian traversable wormholes*, *Class. Quant. Grav.* **38** (2021) 215007 <https://doi.org/10.1088/1361-6382/ac213b>.
- [25] M. Heydari-Fard, M. Heydari-Fard, H.R. Sepangi, *Null geodesics and shadow of hairy black holes in Einstein-Maxwell-dilaton gravity*, *Phys. Rev. D* **105** (2022) 124009 <https://doi.org/10.1103/PhysRevD.105.124009>.
- [26] M. Heydari-Fard and M. Heydari-Fard, *Null geodesics and shadow of 4D Einstein–Gauss–Bonnet black holes surrounded by quintessence*, *Int. J. Mod. Phys. D* **2250066** (2022) 1 <https://doi.org/10.1142/S0218271822500663>.
- [27] A. He, J. Tao, Y. Xue and L. Zhang, *Shadow and photon sphere of black hole in clouds of strings and quintessence*, *Chinese Physics C* **46** (2022) 065102 <https://doi.org/10.1088/1674-1137/ac56cf>.
- [28] J.P. Luminet, *Image of a spherical black hole with thin accretion disk*, *Astron. Astrophys.* **75** (1979) 228
- [29] S.E. Gralla, D.E. Holz and R.M. Wald, *Black hole shadows, photon rings, and lensing rings*, *Phys. Rev. D* **100** (2019) 024018 <https://doi.org/10.1103/PhysRevD.100.024018>.
- [30] P.V.P. Cunha, N.A. Eirco, C.A.R. Herdeiro and J.P.S. Lemos, *Lensing and shadow of a black hole surrounded by a heavy accretion disk*, *JCAP* **03** (2020) 035 <https://doi.org/10.1088/1475-7516/2020/03/035>.
- [31] R. Narayan, M. D. Johnson and C.F. Gammie, *The Shadow of a Spherically Accreting Black Hole*, *ApJ Letter* **885** (2019) L33 <https://doi.org/10.3847/2041-8213/ab518c>.
- [32] X.X. Zeng and H.Q. Zhang, *Influence of quintessence dark energy on the shadow of black hole*, *Eur. Phys. J. C* **80** (2020) 1058 <https://doi.org/10.1140/epjc/s10052-020-08656-7>.
- [33] X.X. Zeng, H.Q. Zhang and H. Zhang, *Shadows and photon spheres with spherical accretions in the four-dimensional Gauss–Bonnet black hole*, *Eur. Phys. J. C* **80** (2020) 872 <https://doi.org/10.1140/epjc/s10052-020-08449-y>.
- [34] S. Guo, K.J. He, G.R. Li and G.P. Li, *The shadow and photon sphere of the charged black hole in Rastall gravity*, *Class. Quant. Grav.* **38** (2021) 165013 <https://dx.doi.org/10.1088/1361-6382/ac12e4>.
- [35] S. Guo, G.R. Li and E.W. Liang, *Influence of accretion flow and magnetic charge on the observed shadows and rings of the Hayward black hole*, *Phys. Rev. D* **105** (2022) 023024 <https://doi.org/10.1103/PhysRevD.105.023024>.
- [36] M. Wang, S. Chen J. Wang and J. Jing, *Shadow of a Schwarzschild black hole surrounded by a Bach Weyl ring*, *Eur. Phys. J. C* **80** (2020) 110 <https://doi.org/10.1140/epjc/s10052-020-7641-3>.
- [37] K. Saurabh and K. Jusufi, *Imprints of dark matter on black hole shadows using spherical accretions*, *Eur. Phys. J. C* **81** (2021) 490 <https://doi.org/10.1140/epjc/s10052-021-09280-9>.

- [38] H.M. Wang, Z.C. Lin and S.W. Wei, *Optical appearance of Einstein-Æther black hole surrounded by thin disk*, <https://doi.org/10.48550/arXiv.2205.13174>.
- [39] S. Kala, Saurabh, H. Nandan and P. Sharma, *Deflection of light and shadow cast by a dual-charged stringy black hole*, *Int. J. Mod. Phys. A* **35** (2020) 2050177 <https://doi.org/10.1142/S0217751X20501778>.
- [40] Y. Hou, Z. Zhang, H. Yan, M. Guo and B. Chen, *Image of Kerr-Melvin black hole with thin accretion disk*, *Phys. Rev. D* **106** (2022) 064058 <https://doi.org/10.1103/PhysRevD.106.064058>.
- [41] S.J. Ma, T.C. Ma, J.B. Deng and X.R. Hu, *Black hole shadow, photon ring and lensing ring in the CDM halo*, <https://doi.org/10.48550/arXiv.2206.12820>.
- [42] O. Donmez, F. Dogan and T. Sahin, *Study of asymptotic velocity in the Bondi-Hoyle accretion flows in the domain of Kerr and 4D Einstein-Gauss-Bonnet gravities*, <https://doi.org/10.48550/arXiv.2205.14382>.
- [43] S. Guo, G.R. Li and E.W. Liang, *Observable characteristics of the charged black hole surrounded by thin disk accretion in Rastall gravity*, *Class. Quant. Grav.* **39** (2022) 135004 <https://dx.doi.org/10.1088/1361-6382/ac6fa8>.
- [44] A. Uniyal, R.C. Pantig and A. Ovgun, *Probing a nonlinear electrodynamics black hole with thin accretion disk, shadow and deflection angle with M87* and Sgr A* from EHT*, *Physics of the Dark Universe* **40** (2023) 101178 <https://doi.org/10.1016/j.dark.2023.101178>.
- [45] M. Guerrero, G.J. Olmo, D. Rubiera-Garcia and D.S.C. Gomez, *Light ring images of double photon spheres in black hole and wormhole spacetimes*, *Phys. Rev. D* **105** (2022) 084057 <https://doi.org/10.1103/PhysRevD.105.084057>.
- [46] X.X. Zeng, K.J. He and G.P. Li, *Effects of dark matter on shadows and rings of brane-world black holes illuminated by various accretions*, *Sci. China Phys. Mech. Astron.* **65** (2022) 290411 <https://doi.org/10.1007/s11433-022-1896-0>.
- [47] A.M. Bauer, A. Cárdenas-Avenidaño, C.F. Gammie and N. Yunes, *Spherical accretion in alternative theories of gravity*, *Astrophys. J.* **925** (2022) 119 <https://doi.org/10.3847/1538-4357/ac3a03>.
- [48] M. Okyay and A. Ovgun, *Nonlinear electrodynamics effects on the black hole shadow, deflection angle, quasi-normal modes and greybody factors*, *JCAP* **01** (2022) 009 <https://doi.org/10.1088/1475-7516/2022/01/009>.
- [49] Q. Gan, P. Wang, H. Wu and H. Yang, *Photon ring and observational appearance of a hairy black hole*, *Phys. Rev. D* **104** (2021) 044049 <https://doi.org/10.1103/PhysRevD.104.044049>.
- [50] M. Guerrero, G.J. Olmo, D. Rubiera-Garcia and D.S.C. Gomez, *Shadows and optical appearance of black bounces illuminated by a thin accretion disk*, *JCAP* **08** (2021) 036 <https://doi.org/10.1088/1475-7516/2021/08/036>.
- [51] K.J. He, S. Guo, S.C. Tan and G.P. Li, *Shadow images and observed luminosity of the Bardeen black hole surrounded by different accretions*, *Chin. Phys. C* **46** (2022) 085106 <https://dx.doi.org/10.1088/1674-1137/ac67fe>.
- [52] X. Qin, S. Chen and J. Jing, *Image of a regular phantom compact object and its luminosity under spherical accretions*, *Class. Quant. Grav.* **38** (2021) 115008 <https://doi.org/10.1088/1361-6382/abf712>.
- [53] R. Shaikh, P. Kocherlakota, R. Narayan and P.S. Joshi, *Shadows of spherically symmetric black holes and naked singularities*, *Mon. Not. R. Astron. Soc.* **482** (2019) 52 <https://doi.org/10.1093/mnras/sty2624>.
- [54] K. Saurabh and K. Jusufi, *Imprints of dark matter on black hole shadows using spherical accretions*, *Eur. Phys. J. C* **81** (2021) 490 <https://doi.org/10.1140/epjc/s10052-021-09280-9>.

- [55] M. Heydari-Fard, S. Ghassemi Honarvar and M. Heydari-Fard, *Thin accretion disk luminosity and its image around rotating black holes in perfect fluid dark matter*, *Mon. Not. R. Astron. Soc.* **521** (2023) 708 <https://doi.org/10.1093/mnras/stad558>.
- [56] A.G. Riess, et al, *Observational evidence from supernovae for an accelerating universe and a cosmological constant*, *Astron. J.* **116** (1998) 1009 <https://doi.org/10.1086/300499>.
- [57] S. Perlmutter, et al, *Measurements of omega and lambda from 42 high-redshift supernovae*, *Astrophys. J.* **517** (1999) 565 <https://doi.org/10.1086/307221>.
- [58] P.J.E. Peebles and B. Ratra, *Cosmology with a time-variable cosmological constant*, *Astrophys. J.* **325** (1988) L17.
- [59] R.R. Caldwell, R. Dave and P.J. Steinhardt, *Cosmological imprint of an energy component with general equation of state*, *Phys. Rev. Lett.* **80** (1998) 1582 <https://doi.org/10.1103/PhysRevLett.80.1582>.
- [60] V. V. Kiselev, *Quintessence and black holes*, *Class. Quant. Grav.* **20** (2003) 1187 <https://doi.org/10.1088/0264-9381/20/6/310>.
- [61] V.V. Kiselev, *Quintessential solution of dark matter rotation curves and its simulation by extra dimensions*, <https://doi.org/10.48550/arXiv.gr-qc/0303031>.
- [62] J.M. Bardeen, *Non-singular general-relativistic gravitational collapse*, Proceedings of the International Conference GR5, Tbilisi, U.S.S.R., 174 (1968).
- [63] E. Ayon-Beato and A. Garcia, *The Bardeen model as a nonlinear magnetic monopole*, *Phys. Lett. B* **493** (2000) 149 [https://doi.org/10.1016/S0370-2693\(00\)01125-4](https://doi.org/10.1016/S0370-2693(00)01125-4).
- [64] S.A. Hayward: *Formation and evaporation of nonsingular black holes*, *Phys. Rev. Lett.* **96** (2006) 031103 <https://doi.org/10.1103/PhysRevLett.96.031103>.
- [65] C. Bambi and L. Modesto, *Rotating regular black holes*, *Phys. Lett. B* **721** (2013) 329 <https://doi.org/10.1016/j.physletb.2013.03.025>.
- [66] V.P. Frolov, *Notes on nonsingular models of black holes*, *Phys. Rev. D* **94** (2016) 104056 <https://doi.org/10.1103/PhysRevD.94.104056>.
- [67] O. Pedraza, L.A. López, R. Arceo and I. Cabrera-Munguia, *Geodesics of Hayward black hole surrounded by quintessence*, *Gen. Relativ. Grav.* **53** (2021) 24 <https://doi.org/10.1007/s10714-021-02798-z>.
- [68] L.L. Shi, J.P. Hu, Y. Zhang, C. Ma and P.F Duan, *Geodesic structure of a non-linear magnetic charged black hole surrounded by quintessence*, *Commun. Theor. Phys.* **71** (2019) 1187 <https://dx.doi.org/10.1088/0253-6102/71/10/1187>.
- [69] A. Benavides-Gallego, A. A. Abdujabbarov and C. Bambi, *Rotating and nonlinear magnetic-charged black hole surrounded by quintessence*, *Phys. Rev. D* **101** (2020) 044038 <https://doi.org/10.1103/PhysRevD.101.044038>.
- [70] P.Z. He, Q.Q. Fan, H.R. Zhang and J.B. Deng, *Shadows of rotating Hayward–de Sitter black holes with astrometric observables*, *Eur. Phys. J. C* **80** (2020) 1195 <https://doi.org/10.1140/epjc/s10052-020-08707-z>.
- [71] R. Kumar, S.G. Ghosh and A. Wang, *Shadow cast and deflection of light by charged rotating regular black holes*, *Phys. Rev. D* **100** (2019) 124024 <https://doi.org/10.1103/PhysRevD.100.124024>.
- [72] C. Sun, Y. Liu, W.L. Qian and R. Yue, *Shadows of magnetically charged rotating black holes surrounded by quintessence*, *Chin. Phys. C* **46** (2022) 065103 <https://doi.org/10.1088/1674-1137/ac588c>.
- [73] Y. Huang, S. Chen and J. Jing, *Double shadow of a regular phantom black hole as photons couple to the Weyl tensor*, *Eur. Phys. J. C* **76** (2016) 594 <https://doi.org/10.1140/epjc/s10052-016-4442-9>.

- [74] A. Belhaj, H. Belmahi, M. Benali, H. El Moumni, M. A. Essebani and M.B. Sedra, *Optical shadows of rotating Bardeen-AdS black holes*, *Mod. Phys. Lett. A* **37** (2022) 2250032 <https://doi.org/10.1142/S0217732322500328>.
- [75] Z. Stuchlik and J. Schee, *Shadow of the regular Bardeen black holes and comparison of the motion of photons and neutrinos*, *Eur. Phys. J. C* **79** (2019) 44 <https://doi.org/10.1140/epjc/s10052-019-6543-8>.
- [76] C. Bambi: *Black Holes A Laboratory for Testing Strong Gravity*, Springer, (2017) <https://doi.org/10.1007/978-981-10-4524-0>.
- [77] K. Jusufi, K., A. Ovgun, J. Saavedra, Y. Vasquez, and P.A. Gonzalez, *Deflection of light by rotating regular black holes using the Gauss-Bonnet theorem*, *Phys. Rev. D* **97** (2018) 124024 <https://doi.org/10.1103/PhysRevD.97.124024>.
- [78] W. Javed, J. Abbas and A. Ovgun, *Effect of the quintessential dark energy on weak deflection angle by Kerr-Newmann black hole*, *Annals Phys.*, **418** (2020) 168183 <https://doi.org/10.1016/j.aop.2020.168183>.
- [79] H. Shiyang, L. Chen Deng Dan, W. Xin and E. Liang, *Observational signatures of Schwarzschild-MOG black holes in scalar-tensor-vector gravity: shadows and rings with different accretions*, *Eur. Phys. J. C* **82** (2022) 885 <https://doi.org/10.1140/epjc/s10052-022-10868-y>.
- [80] V. Perlick and O.Y. Tsupko, *Calculating black hole shadows: review of analytical studies*, *Phys. Rep.*, **947** (2022) 1 <https://doi.org/10.3847/1538-4357/aca58a>.
- [81] Y. Mizuno, Z. Younsi and C.M. Fromm, et al. *The current ability to test theories of gravity with black hole shadows*, *Nat. Astron.* **2** (2018) 585 <https://doi.org/10.1038/s41550-018-0449-5>.
- [82] D. Psaltis, *Testing general relativity with the Event Horizon Telescope*, *Gen. Relativ. Grav.* **51** (2019) 137 <https://doi.org/10.1007/s10714-019-2611-5>.
- [83] A. Stepanian, S. Khlgatyan and V.G. Gurzadyan, *Black hole shadow to probe modified gravity*, *Eur. Phys. J. Plus* **136** (2021) 127 <https://doi.org/10.1140/epjp/s13360-021-01119-2>.
- [84] Z. Younsi, D. Psaltis and F. Özel, *Black hole images as tests of general relativity: effects of spacetime geometry*, *Astrophys. J.* **942** (2023) 1 <https://doi.org/10.3847/1538-4357/aca58a>.
- [85] R.K.Walia, S.G.Ghosh and S.D. Maharaj, *Testing rotating regular metrics with EHT results of Sgr A**, *Astrophys. J.* **939** (2022) 2 <https://doi.org/10.3847/1538-4357/ac9623>.
- [86] S. Vagnozzi, R. Roy and Y.D. Tsai, et al. *Horizon-scale tests of gravity theories and fundamental physics from the Event Horizon Telescope image of Sagittarius A**, [arXiv:2205.07787 [gr-qc]].
- [87] M. Jaroszynski and A. Kurpiewski, *Optics near Kerr black holes: spectra of advection dominated accretion flows*, *Astron. Astrophys.* **326** (1997) 419 [arXiv:astro-ph/9705044].
- [88] C. Bambi, *Can the supermassive objects at the centers of galaxies be traversable wormholes? The first test of strong gravity for mm/sub-mm very long baseline interferometry facilities*, *Phys. Rev. D* **87** (2013) 107501 <https://doi.org/10.1103/PhysRevD.87.107501>.